A&A 402, 653–666 (2003)
DOI: 10.1051/0004-6361:20030119

Astronomy & Astrophysics

XMM-Newton high-resolution X-ray spectroscopy of the Wolf-Rayet object WR 25 in the Carina OB1 association⋆

A. J. J. Raassen[1,2], K. A. van der Hucht[1], R. Mewe[1], I. I. Antokhin[3,4,5], G. Rauw[3,⋆⋆], J.-M. Vreux[3], W. Schmutz[6], and M. Güdel[7]

[1] SRON National Institute for Space Research, Sorbonnelaan 2, 3584 CA Utrecht, The Netherlands
e-mail: a.j.j.raassen@sron.nl;k.a.van.der.hucht@sron.nl;r.mewe@sron.nl
[2] Astronomical Institute Anton Pannekoek, Kruislaan 403, 1098 SJ Amsterdam, The Netherlands
e-mail: raassen@astro.uva.nl
[3] Institut d'Astrophysique et de Géophysique, Université de Liège, Allée du 6 Août, 17 Bât. B5c, 4000 Liège, Belgique
e-mail: rauw@astro.ulg.ac.be; vreux@astro.ulg.ac.be
[4] *Present address*: Department of Physics and Astronomy, University of Glasgow, Kelvin Building, Glasgow G12 8QQ, Scotland, UK
e-mail: igor@astro.gla.ac.uk
[5] On leave from: Sternberg Astronomical Institute, Moscow University, Universitetskij Prospect 13, Moscow 119899, Russia
[6] Physikalisch-Meteorologisches Observatorium Davos, Dorfstrasse 33, 7260 Davos Dorf, Switzerland
e-mail: w.schmutz@pmodwrc.ch
[7] Paul Scherrer Institut, Würenlingen & Villigen, 5232 Villigen PSI, Switzerland
e-mail: guedel@astro.phys.ethz.ch

Received 26 November 2002 / Accepted 21 January 2003

Abstract. We report the analysis of the first high-resolution X-ray spectra of the Wolf-Rayet (WR) object WR 25 (HD 93162, WN6ha+O4f) obtained with the Reflection Grating Spectrometers (RGS) and the European Photon Imaging Cameras (EPIC-MOS and PN) CCD spectrometers on board the *XMM-Newton* satellite. The spectrum exhibits bright emission lines of the H- and He-like ions of Ne, Mg, Si and S, as well as Fe XVIII to Fe XX and Fe XXV lines. Line fluxes have been measured. The RGS and EPIC spectra have been simultaneously fitted to obtain self-consistent temperatures, emission measures, and elemental abundances. Strong absorption by the dense WR stellar wind and the interstellar medium (ISM) is observed equivalent to $N_{\rm H} = 7{\times}10^{21}$ cm^{-2}. Multi-temperature (DEM) fitting yields two dominant components around temperatures of 7.0 and 32 MK, respectively. The *XMM* intrinsic (i.e. unabsorbed, corrected for the stellar wind absorption and the absorption of ISM) X-ray luminosity of WR 25 is $L_{\rm x}(0.5\text{–}10\ {\rm keV}) = 1.3 \times 10^{34}$ erg s^{-1}, and $L_{\rm x}(0.5\text{–}10\ {\rm keV}) = 0.85 \times 10^{34}$ erg s^{-1}, (when correcting for the ISM only) assuming $d = 3.24$ kpc. The obtained chemical abundances are subsolar, except for S. This may be real, but could equally well be due to a weak coupling to the continuum, which is strongly influenced by the absorption column density and the subtracted background. The expected high N-abundance, as observed in the optical wavelength region, could not be confirmed due to the strong wind absorption, blocking out its spectral signature. The presence of the Fe XXV emission-line complex at ~ 6.7 keV is argued as being indicative for colliding winds inside a WR+O binary system.

Key words. stars: individual: WR 25 – stars: early-type – stars: Wolf-Rayet – stars: binaries: general – stars: abundances – X-rays: stars

1. Introduction

Wolf-Rayet (WR) stars represent the one-but last phase in the evolution of massive stars with $M_{\rm i} \gtrsim 20\,M_{\odot}$. For a review on WR stars see, e.g., van der Hucht (1992).

The first report of X-ray emission by a WR star is from Seward et al. (1979), who presented *Einstein* X-ray (0.2–4.0 keV) observations of the Carina open cluster Tr 16 and its environment, including six O-type stars and one WR star, WR 25 (HD 93162, Tr16-177, WN6h+O4f; WR catalog number and spectral type from van der Hucht et al. 1981 and van der Hucht 2001). Subsequent *Einstein* observations by Seward & Chlebowski (1982) of the same region show X-rays from 15 O-type and WR stars. The data are consistent with the hypothesis that $L_{\rm x} \simeq 2.0 \times 10^{-7}\,L_{\rm bol}$ for all O-type stars in this region with remarkably little scatter. Yet, WR 25 had $L_{\rm x} \simeq 20 \times 10^{-7}\,L_{\rm bol}$, a factor of 30 larger than for the other WR

Send offprint requests to: A. J. J. Raassen,
e-mail: a.j.j.raassen@sron.nl

⋆ Based on observations obtained with *XMM-Newton*, an ESA science mission with instruments and contributions directly funded by ESA Member States and the USA (NASA).

⋆⋆ Research Associate FNRS (Belgique).

stars in this region: WR 22 (HD 92740, WN7ha+O9III-V) and WR 24 (HD 93131, WN6ha). Adopting all to be at a heliocentric distance of $d = 2.6$ kpc, they found for WR 22, WR 24 and WR 25 that $L_x \simeq 3.6$, <2.5 and 73.8×10^{32} erg s^{-1}, respectively. *Einstein* observations of other WR stars (Sanders et al. 1985; White & Long 1986) showed $L_x / L_{bol} \simeq 10^{-7}$ with considerable scatter, but leaving WR 25 exceptionally bright in X-rays compared with WR stars of various different subtypes.

Subsequent X-ray observations of WR stars by the *EXOSAT*, *Ginga*, *ROSAT* and *ASCA* satellite observatories have added considerably to the X-ray view of WR stars. For X-ray surveys of large samples of WR stars, see Pollock (1987) and Pollock et al. (1995). For reviews on X-ray properties of WR stars see, e.g., Willis & Crowther (1996), van der Hucht (2002b), and Corcoran (2003).

A uniform analysis of all 48 WR stars positively detected with *Einstein* (Pollock 1987) showed that their X-ray luminosities cover a range of more than two orders of magnitude. In particular: *(i)* single WN stars exhibit L_x-values of about a factor of four larger than do single WC stars; *(ii)* WR+OB binary systems tend to be X-ray brighter than single WR stars; and *(iii)* the few WR stars with absorption lines in their spectra appear significantly more X-ray luminous than single WR stars, an indication that they may be WR+OB binaries. *ROSAT* observations of some 150 galactic WR stars confirm and detail this view (Pollock et al. 1995).

The X-ray-brightest Galactic WR object detected to date is WR 43c (HD 97950-C, WN6ha+?, period hundreds of days, Moffat & Niemela 1984) in the cluster NGC 3603, with a *Chandra*-ACIS-I (0.3–10 keV) unabsorbed X-ray luminosity of $L_x \approx 8{\times}10^{34}$ erg s^{-1} (Moffat et al. 2002).

X-rays may be either of thermal or non-thermal origin. Assuming a thermal generation, the observed X-rays indicate temperatures of a few million degrees Kelvin. Such temperatures are not expected in the atmospheres of these hot (~30–90 kK) stars as long as radiative equilibrium holds. Thus some material must be heated by non-radiative energy transfer, e.g., by hydrodynamic shocks. In WR binaries with a massive companion these shocks may arise from colliding winds, whereas in systems with a compact companion shocks could be caused by accretion phenomena. For single WR stars, however, those shocks must be an intrinsic property of the stellar wind.

According to the phenomenological model proposed by Lucy & White (1980) and further elaborated by Lucy (1982), shocks are generated throughout a radiation driven stellar wind as the consequence of dynamical instabilities. Such instabilities have been studied in detail by, e.g., Owocki & Gayley (1995, 1999), Owocki & Cohen (1999) and Dessart & Owocki (2002). Model computations predict shock velocity-jumps ranging from 500 to 1000 km s^{-1}, implying post-shock temperatures which could account for the observed thermal X-ray production. The Owocki et al. models were developed for the radiation-driven winds of OB stars, while the driving mechanism of the stronger mass-loss from WR stars is not yet established. Baum et al. (1992) have modeled the observed X-ray emission of WR stars in a semi-empirical approach , assuming a standard non-LTE WR model-atmosphere component in radiative equilibrium and a hot component of shocked material, homogeneously distributed throughout the WR atmosphere, accounting for the free-free absorption of X-rays and their non-LTE transfer. The model of Baum et al. can reproduce the low-level WR X-ray fluxes, assuming a temperature of about 4×10^6 K and a filling factor of a few percent in terms of the mass. The observed X-rays are emerging from far out in the stellar wind, due to the large optical depths. Further modeling of X-rays from single stars is provided by, e.g., Feldmeier et al. (1997a,b), Ignace et al. (2000) and Ignace & Gayley (2002).

Table 1. Stellar parameters of WR 25.

quantity		value	ref.
spectral type		WN6h+O4f	1
d	(kpc)	3.24	1
v	(mag)	8.14	1
$b - v$	(mag)	0.17	1
M_v	(mag)	–6.20	1
A_v	(mag)	1.79	1
E_{b-v}	(mag)	0.44	1
E_{B-V}	(mag)	0.53	1
v_∞	(km s^{-1})	2480	1
T_*	(kK)	31	2
log $L/L_\odot$		5.97	2
$\dot{M}$	(10^{-5} $M_\odot$ yr^{-1})	3.6	2

References: 1) van der Hucht (2001); 2) Crowther et al. (1995a).

In the case of WR binaries, Cherepashchuk (1976) and Prilutskii & Usov (1976) developed the idea that the collision of two supersonic winds in a WR+O binary system should cause a bright, extensive X-ray temperature shock to form between them. Therefore, OB+OB and WR+OB binaries do not only add X-rays generated in the individual binary components, but provide also an additional X-ray excess due to the collision of the stellar winds of the binary components (e.g., Luo et al. 1990; Stevens et al. 1992; Pittard & Stevens 1997, 2002).

X-ray transitions involve the innermost atomic electrons and thus, in principle, provide a means of assessing chemical abundances, via both thermal emission-line and photoelectric-absorption-edge spectra between 0.1 and 10 keV, that is not compromised by the difficulties at longer wavelengths concerning ionization balance (Pollock 1995). They are thus of special relevance to the study of the WR stars that are generally accepted to be chemically evolved.

As mentioned above, WR 25 had the most prominent WR *Einstein* X-ray emission excess. Also its *ROSAT* X-ray flux is among the larger ones for WR stars. Its X-ray luminosity excess is suggestive of a colliding-wind binary with a very long period ($P \gtrsim 10$ yr), like WR 140 (Pollock 1989; Williams et al. 1990; van der Hucht et al. 1992; Corcoran et al. 1995).

Seward & Chlebowski (1982) derived from the *Einstein* (0.2–4.0 keV) data of WR 25, assuming a thermal model and $d = 2.6$ kpc, that $L_x \simeq 73.8 \times 10^{32}$ erg s^{-1}. Pollock (1987) reanalyzed the *Einstein* (0.2–4.0 keV) data of WR 25, also assuming a thermal spectrum, of 1 keV, and $d = 2.6$ kpc, found that $L_x \simeq 137 \times 10^{32}$ erg s^{-1}. This over-estimation is due to extrapolation of the 1 keV thermal spectrum from the hard IPC band to the soft one, neglecting wind absorption (see Sect. 4.3).

Table 2. Log of WR 25 observations by *XMM-Newton*.

revolution	#115	#116	#283	#284	#285
obs. date	26-7-2000	27-7-2000	25-6-2001	28-6-2001	30-6-2001
start [UT]	04:58	23:48	06:51	07:22	04:38
instrument	integration time (hr)				
RGS 1	-	-	10.3	11.8	10.5
RGS 2	-	-	10.3	11.8	10.5
MOS 1	9.4	3.1	10.2	11.7	10.4
MOS 2	8.5	2.3	10.2	11.7	10.4
PN	8.8	2.6	9.6	11.0	9.7

ROSAT (0.2–2.4 keV) data for WR 25 yielded, again assuming $d = 2.6$ kpc, $L_x \simeq 49 \times 10^{32}$ erg s^{-1} (Pollock et al. 1995; corrected by Wessolowski 1996).

ASCA (0.5–4 keV) data discussed by Skinner et al. (1995) showed no significant variability within 11 hr, and a relatively soft spectrum with a *Bremsstrahlung*-model fit of $kT \simeq 1.6$ keV and very little emission above 2 keV. Its derived X-ray luminosity, assuming $d = 2.6$ kpc, is $L_x \simeq 20 \times 10^{32}$ erg s^{-1}.

The different results demonstrate the need for a homogeneous analysis of all archive data of WR 25, as performed in Sect. 4.

Basic stellar parameters of WR 25 are listed in Table 1. The binary nature of WR 25 is still a matter of debate. WR 25 combines a *diluted* WN6-7 emission-line spectrum (e.g., Walborn et al. 1985) with a strong early-type absorption spectrum. H. Smith (1955) assigned a WN7+O7 spectral type, confirmed by L. F. Smith (1968). Subsequently, WR 25 has been classified WN6-A by Walborn (1974), WN7+a by van der Hucht et al. (1981) and WN6ha by L. F. Smith et al. (1996), due to lack of a radial velocity solution (but this could equally well indicate either a single star status, or a pole-on binary orbit, or a very long period). For the same reason, Moffat (1978) and Conti et al. (1979) rejected a binary status, although the former noted that the absorption component in the optical spectrum of WR 25 corresponds to an O4f spectral type. Van der Hucht (2001), on the basis of the diluted emission lines in the UV spectrum of WR 25 published by Walborn et al. (1985) and the absorption-component spectral type given by Moffat (1978), provocatively settled on WN6h+O4f, the spectral type which we adopt also here. Prinja et al. (1990) determined for single WN6 stars C IV-wind terminal velocities averaging ~1700 km s^{-1}, while for WR 25 they find 2500 km s^{-1}, a C IV-wind terminal velocity common for O4 stars. Drissen et al. (1992) found optical polarization variability in WR 25 and suggested that this could be binary-induced in case of a long-period (years) orbit. Van der Hucht et al. (1992) emphasized the correlation between excess X-ray luminosities and non-thermal radio emission for a number of long-period WR binaries. At radio wavelengths, WR 25 has been detected to date only at 3 cm (Leitherer et al. 1995; Chapman et al. 1999). Anyhow, the excess X-ray luminosity of WR 25 makes it a colliding-wind-binary candidate of considerable interest (see also Pollock 1987, 1991), and worthy of multi-frequency long-term monitoring.

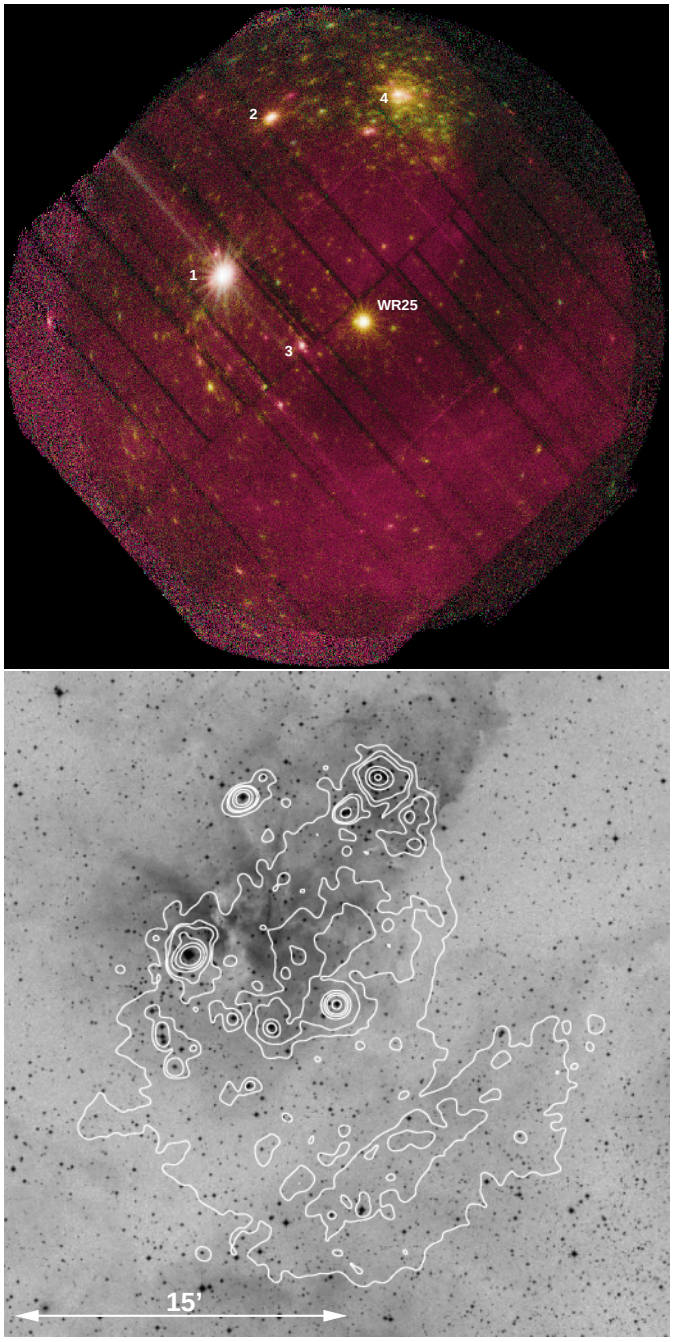

Fig. 1. *Top: XMM* false-color image ($30' \times 30'$) of the WR 25 field from the combined MOS1, MOS2 and PN exposures in revs. #283, #284, and #285. Axes correspond to RA and Dec. Energy bands selected to create this image are: 0.4–1.0 keV, 1.0–2.5 keV, and 2.5–12.0 keV. Labeled bright sources in the field are: 1: η Car (pec); 2: HD 93250 (O3.5 V((f$^+$))), Walborn et al. 2002); 3: HD 93205 (O3V+O8V); and 4: HD 93129A (O2 If*, Walborn et al. 2002) in the open cluster Tr 14. Numerous fainter X-ray sources are present, many of them also early-type massive stars. Also diffuse emission is visible. *Bottom: XMM*-MOS1 (rev. #284) contours, plotted over an optical Digitized Sky Survey image.

The here presented *XMM-Newton* RGS and EPIC observations of WR 25 allow an improvement of the determination of its X-ray luminosity and a first independent abundance determination of the elements Ne, Mg, Si, S and Fe. The observed element

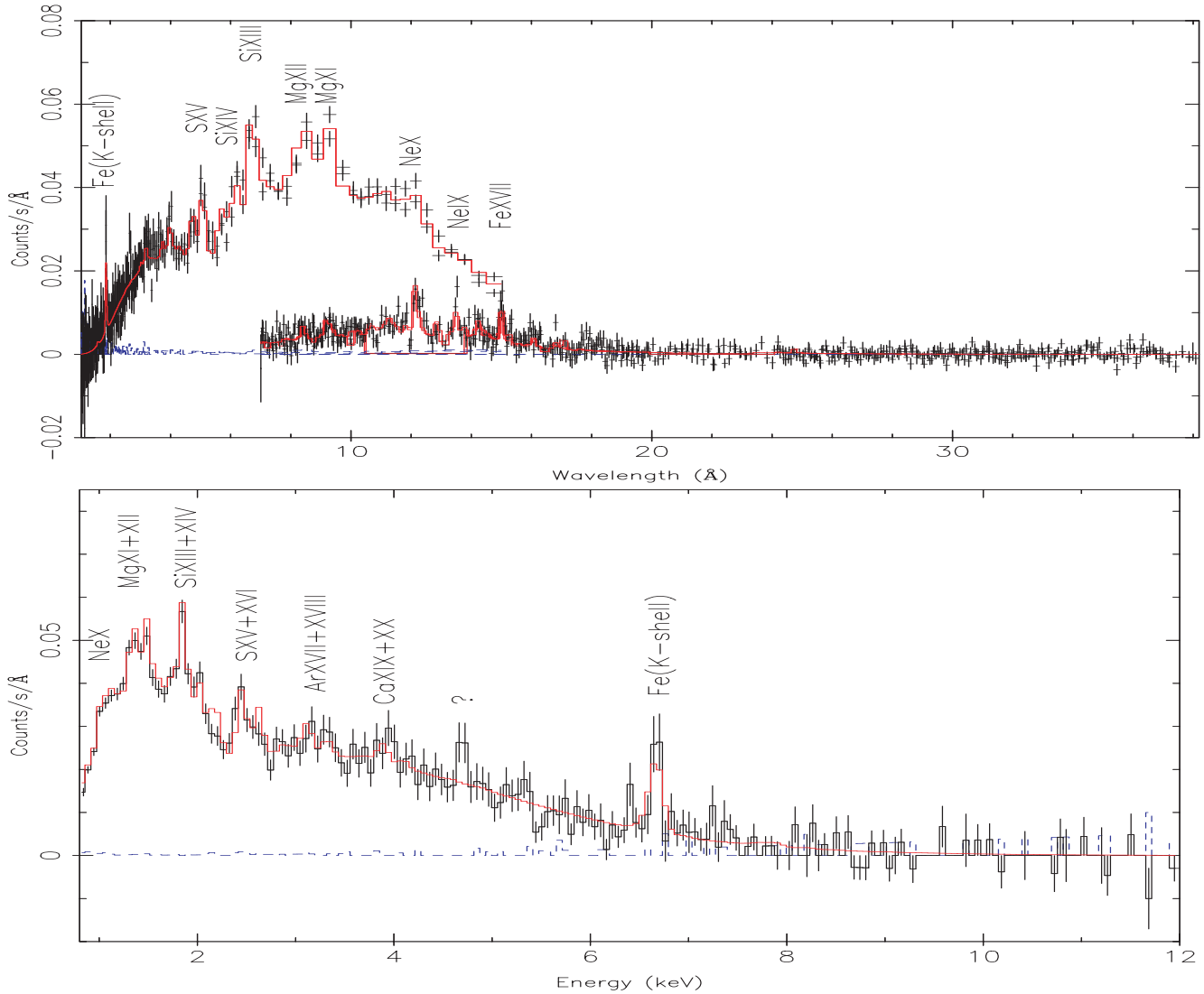

Fig. 2. *Top:* first-order background-subtracted spectra of WR 25 of rev. 284 and 285, observed by *XMM*-RGS (5–38 Å) and *XMM*-EPIC-MOS (1–15 Å). The spectra are not corrected for the effective areas of the instruments, in order to show the different efficiencies. Several prominent lines are labelled with the emitting ions. Note the small error bars. The red line shows the best-fit model and the blue line the subtracted background. Due to the higher resolution the lines above 10 Å are more prominent in the RGS spectrum. The oxygen edge at 23 Å is invisible due to lack of flux for $\lambda \gtrsim 20$ Å. *Bottom:* the *XMM*-EPIC-MOS spectrum of rev. 284. The question mark indicates an unknown emission, which happens to be located at the position of Ti K-shell lines. The cosmic Ti-abundance, however, is low and no other confirmations for the presence of Ti have been found in the spectrum.

ionization stages (cf. Table 3) place constraints on the structure of the X-ray forming regions of the star, and provide tests for understanding the nature of the source of X-ray emission from this Wolf-Rayet star/binary.

2. Observations and data reduction

The *XMM* spectra of WR 25 were recorded with the Reflection Grating Spectrometers (RGSS) and the European Photon Imaging Camera (EPIC) CCD detectors. The log of *XMM* observations of WR 25 is given in Table 2. For general information on *XMM-Newton* and its X-ray instruments, see Jansen et al. (2001), den Herder et al. (2001), Strüder et al. (2001) and Turner et al. (2001). The RGS covers the wavelength range 5 to 35 Å with a resolution of about 0.07 Å (corresponding to velocities of 4200 to 600 km s^{-1}), and a maximum effective area of about 140 cm^2 around 15 Å. The first spectral order has been selected by means of the energy resolution of the CCD detectors (see den Herder et al. 2001). The data were processed with the *XMM-Newton* science analysis software (SAS, version [5.3.3]) system. For *XMM*-RGS the spectrum was extracted including 95% of the cross-dispersion. The background spectrum was obtained by taking events from a region spatially offset from the source, excluding 98%. For the *XMM*-MOS1 the spectrum was obtained by means of extracting the events within a circle around the source with outer radius of 40″. The background was subtracted by means of an annulus centered on the source with inner radius of 50″ and outer radius of 64″.

Table 3. WR 25 emission-line wavelengths and fluxes as observed with *XMM* RGS1 + 2 and EPIC-MOS. Values within parentheses are the 1 σ uncertainties.

RGS1 + RGS2		EPIC-MOS		identification[a]			
λ(Å)	flux[b]	λ(Å)	flux[b]	λ(Å)	E (keV)	ion	type[c]
—	—	1.86	0.05	1.87	6.63	Fe XXV	Kα
—	—	3.98	0.04	3.97	3.12	S XVI	Lyβ
				3.97	3.12	Ar XVII	He4
—	—	5.08	0.15(.03)	5.04	2.45	S XV	He4
—	—	5.7	—	5.64	2.20	Si XIII	He3
—	—	6.2	0.14(.03)	6.20	2.00	Si XIV	Lyα
6.726(.037)	0.53(.25)	6.67	0.40(.05)	6.688	1.853	Si XIII	He4
8.295(.028)	0.13(.07)	8.43	0.14(.04)	8.315	1.491	Fe XXIV	Li3-13
8.424(.032)	0.17(.08)			8.421	1.472	Mg XII	Lyα
9.224(.037)	0.19(.11)	9.22	0.17(.04)	9.170	1.352	Mg XI	He4
9.412(.050)	0.16(.11)			9.3	1.08	Fe-L	
12.136(.064)	0.32(.22)	—	—	12.134	1.022	Ne X	Lyα
13.476(.041)	0.28(.09)	—	—	13.448	0.922	Ne IX	He4
				13.467	0.921	Fe XIX	O1-74
14.251(.028)	0.20(.09)	—	—	14.260	0.869	Fe XVIII	F1-56, 55, 52
14.974(.021)	0.30(.09)	—	—	15.013	0.826	Fe XVII	Ne1-27
15.236(.032)	0.14(.08)	—	—	15.265	0.812	Fe XVII	Ne1-23
15.989(.032)	0.14(.07)	—	—	16.002	0.775	Fe XVIII	F1-4
16.791(.023)	0.19(.08)	—	—	16.780	0.738	Fe XVII	Ne1-5
17.115(.069)	0.08(.07)	—	—	17.055	0.727	Fe XVII	Ne1-3
				17.100	0.725	Fe XVII	Ne1-2

Notes: [a] Identifications from Kelly (1987). [b] Observed average fluxes at Earth in 10^{-4} photon cm^{-2} s^{-1}. No significant differences between line fluxes of rev. 284 and rev. 285 have been noticed. [c] For notation see Mewe et al. (1985), Phillips et al. (1999), and Note 1 of Sect. 3.2.

A check on solar flare protons resulted in the deletions of part of the exposure time (see Table 5). Figure 1a shows a combined *XMM*-EPIC false-color image of the WR 25 field; Fig. 1b shows a X-ray contour diagram, derived from EPIC-MOS1 data of rev. 284, overplotted on an optical DDS image.

Besides WR 25, the EPIC images reveal a number of discrete X-ray sources, most of which are associated with massive stars in the Carina complex. The Carina region harbors several very young open clusters (Trumpler 14, 15 and 16, Collinder 228 and 232) that are extremely rich in very hot and massive stars, and have varying and anomalous extinction (e.g., Thé et al. 1980; Massey & Johnson 1993; and in: Niemela et al. 1995), although some other investigators find the extinction normal (e.g., Turner & Moffat 1980; Drissen et al. 1992). Many of the objects seen in Fig. 1 were already among the first early-type stars discovered to be X-ray sources with *Einstein*. The observed diffuse X-ray emission from the Carina Nebula is probably due to the combined action of the stellar winds of the early-type stars on the ambient interstellar medium. The properties of the discrete sources and the diffuse emission in the Carina Nebula will be discussed in a forthcoming paper.

3. Spectral analysis

3.1. Emission-line identification, line fluxes

Figure 2 shows a superposition of the *XMM*-RGS and -EPIC-MOS spectra, together with the best-fit model spectrum.

In Table 3 we list the wavelengths and fluxes of the emission lines measured with the RGS and the EPIC-MOS instruments. Prominent emission lines are Fe XXV (1.87 Å), S XV (5.04 Å), Si XIII (5.64 Å), Si XIV (6.20 Å), Si XIII (6.65 Å), Mg XII (8.42 Å), Mg XI (9.17 Å) in EPIC-MOS and RGS, and Ne X (12.13 Å), Ne IX (13.45 Å), Fe XVII (15.01 Å), Fe XVII (16.78 Å), Fe XVII (17.10 Å) in RGS-spectra only. Above this wavelength the emitted spectrum is strongly absorbed by the dense stellar wind of the Wolf-Rayet star, equivalent to $N_{\rm H} \gtrsim 2{\times}10^{21}$ cm^{-2} (Cruddace et al. 1974).

We use the term *equivalent* $N_{\rm H}$ here, because the WR 25 WN6 wind consists for ~20% of helium (Crowther et al. 1995a). In WC stars the wind consists mostly of helium, and WC+O binaries show spectacular periodic changes in the equivalent $N_{\rm H}$ during their orbit, e.g., WR 140 (Williams et al. 1990) and WR 11 (Dumm et al. 2003).

We note also that the winds of early-type star are ionized and the cross sections for photoelectric absorption are modified compared to neutral material (see, e.g., Waldron et al. 1998).

The stronger spectral lines have been measured individually by folding monochromatic delta functions through the instrumental response functions in order to derive the integrated line fluxes. A constant "background" level was adjusted in order to account for the real continuum and for the pseudo-continuum created by the overlap of several weak, neglected lines. We notice that below 14 Å the spectrum is dominated by

H-like and He-like transitions of Ne, Mg, Si, S, and above 14 Å by Fe XVII and Fe XVIII lines.

3.2. Global fitting and emission measure modeling

3.2.1. Multi-temperature fitting

We have determined the thermal structure and the elemental composition of WR 25's X-ray emitting plasma by means of multi-temperature fitting and DEM-modeling to the spectrum as a whole. We fitted multi-T optically thin plasma models of the spectra (RGS+MOS) using SPEX (Kaastra et al. 1996a) in combination with the MEKAL (Mewe-Kaastra-Liedahl) code as developed by Mewe et al. (1985, 1995). The MEKAL data base is given as an extended list of fluxes of more than 5400 spectral lines, and is available on the www[1]. From both methods a two-temperature range of plasma activity is obtained. In the multi-temperature calculations we used two temperatures which were spontaneously found by the fitting procedure. The two temperature components were coupled to two different $N_{\rm H}$ absorption column densities, which were free to vary. The temperatures and the corresponding EM values are given in Table 4, together with X-ray luminosities, abundances, and statistical $1\,\sigma$ uncertainties. The luminosities are model luminosities at place of emitting plasma, i.e., corrected for absorption by the ISM and by the dense stellar wind of the Wolf-Rayet star. The abundances are relative to solar photospheric values from optical studies (Anders & Grevesse 1989) except for Fe, for which we use $\log A_{\rm Fe} = 7.50$[2] (see Grevesse & Sauval 1998 and 1999) instead of 7.67 (Anders & Grevesse 1989).

From Table 4 we notice that the emission from the "cool" component (7 MK) faces the high absorbing column density, while the emission from the "hot" region (33 MK) is coupled to the low $N_{\rm H}$ value. This indicates that the "hot" component is formed higher up in the wind. The same was noticed by Pollock (2002) based on Doppler shifts and Doppler broadening of lines in the spectrum of the Wolf-Rayet binary WR140 (WC7+O4-5). The emission measure of the low temperature component is higher than that of the high temperature. The latter is highly responsible for the Fe XXV line and the hot continuum, observed by *XMM*-EPIC-MOS. The obtained values of observations during revs. 284 and 285 are very well comparable. No change in physical conditions have been established between the two observations.

Table 4. Multi-temperature fitting for *XMM* spectra of WR 25.

parameter	rev. #284	rev. #285
d (kpc) assumed	3.24	3.24
$N_1^{\rm H}$ (10^{21} cm^{-2})	7.7 ± 0.6	6.3 ± 0.6
$N_2^{\rm H}$ (10^{21} cm^{-2})	2.4 ± 0.7	3.2 ± 0.6
T_1 (MK)	7.1 ± 0.3	6.9 ± 0.3
T_2 (MK)	33 ± 4	30 ± 2
EM_1 (10^{56} cm^{-3})	7.4 ± 1.1	6.1 ± 0.9
EM_2 (10^{56} cm^{-3})	3.0 ± 0.5	2.6 ± 0.2
$L_{\rm x}$ [0.5–10 keV] (10^{32} erg s^{-1})	128 ± 14	129 ± 12
Abundances[a]:		
He	2.27[b]	2.27[b]
C	0.15[b]	0.15[b]
N	5.9[b]	5.9[b]
O	<0.4	<0.24
Ne	$0.54^{+0.15}_{-0.15}$	$0.48^{+0.11}_{-0.11}$
Mg	$0.67^{+0.09}_{-0.09}$	$0.58^{+0.08}_{-0.08}$
Si	$0.83^{+0.10}_{-0.10}$	$0.86^{+0.10}_{-0.10}$
S	$1.3^{+0.2}_{-0.2}$	$1.1^{+0.2}_{-0.2}$
Fe_1	$0.56^{+0.05}_{-0.05}$	$0.40^{+0.03}_{-0.03}$
Fe_2	$0.64^{+0.14}_{-0.14}$	$0.62^{+0.10}_{-0.10}$
$\chi^2_{\rm red}$	643/619	727/613

Notes:
$L_{\rm x}$ values unabsorbed i.e., corrected for absorption by the ISM and stellar wind.
[a] Relative to solar photospheric number abundances (Anders & Grevesse 1989 or Grevesse & Sauval 1998 and 1999 for Fe).
[b] Fixed on literature values given in Sect. 3.2.2.

3.2.2. Abundance determination

Based on the optical spectrum Crowther et al. (1995a) derived abundance values for H/He = 4.5 (number ratio), while Crowther et al. (1995b) added that N/He = 0.003 and C/He = 0.00024. The H/He ratio shows a H-depletion by a factor of about two compared to standard solar photospheric abundances from Anders & Grevesse (1989). This H-depletion was confirmed by Hamann & Koesterke (1998). No optical O-abundance is available in the literature. Due to the high $N_{\rm H}$ values, resulting in strong absorption above 15 Å, no C, N, and O-lines have been measured from our X-ray spectra, and therefore no abundance values can be obtained here for those elements. For He, C, and N, the abundance values obtained by Crowther et al. (1995a,b) in the optical wavelength range have been adopted. For O only an upper limit could be determined. This value might be biased by the strong absorption.

For the other elements (Ne, Mg, Si and Fe, except S) the obtained values are all subsolar. This might be real but could equally well be due to a weak coupling to the continuum, which is strongly influenced by the absorption column density and subtracted background. The relative (to each other) abundances for these elements, however, are close to solar-like values. Except for Fe, the abundance of the elements are coupled for the two temperature components. The Fe-features, however, are strongly separated in temperature regime (Fe XVII at 7 MK only, and Fe XXV at 32 MK only). Therefore the abundances for these ions were de-coupled and different Fe-abundances were obtained for the two temperature components. These differences, however, are not significant when

[1] `http://www.sron.nl/divisions/hea/spex/version1.10/line/`

[2] Here $\log A_{\rm Fe}$ is the logarithm of the Fe-abundance relative to $\log A_{\rm H} = 12.0$.

the uncertainties in the values are taken into account. To avoid the influence of wavelength shift between the observed data and the model we checked our obtained values by determining abundances based on individual lines. No significant deviations from the values derived in the global fit occur.

3.2.3. Differential emission measure (DEM) modeling

To show the connectivity of the different temperature components we applied a differential emission measure (DEM) model of WR 25's X-ray emitting plasma using the various inversion techniques offered by SPEX (see Kaastra et al. 1996b). We define the DEM by $n_e n_H dV/d\log T$ or integrated over one temperature bin: $EM = n_e n_H V$, where n_e and n_H are the electron and hydrogen density, respectively. In Fig. 3 we show the resulting DEM as a result from simultaneous fitting of the RGS and EPIC spectra of revolutions #284 and #285 with the regularization algorithm (top panel) and with a polynomial fit of order 8 (bottom panel) (see Kaastra et al. 1996b). We assume the same abundances as were obtained in the 2-T fit (Table 4). Although the shapes of the two methods are slightly different, the results are indistinguishable from each other in view of the statistical uncertainties. As can be seen, the emission is concentrated in two temperature intervals around 8 MK and 35 MK with total integrated emission measures of 7.1 and 2.5×10^{56} cm^{-3}, respectively. The emission measures compare well with the values obtained from the multi-temperature fit.

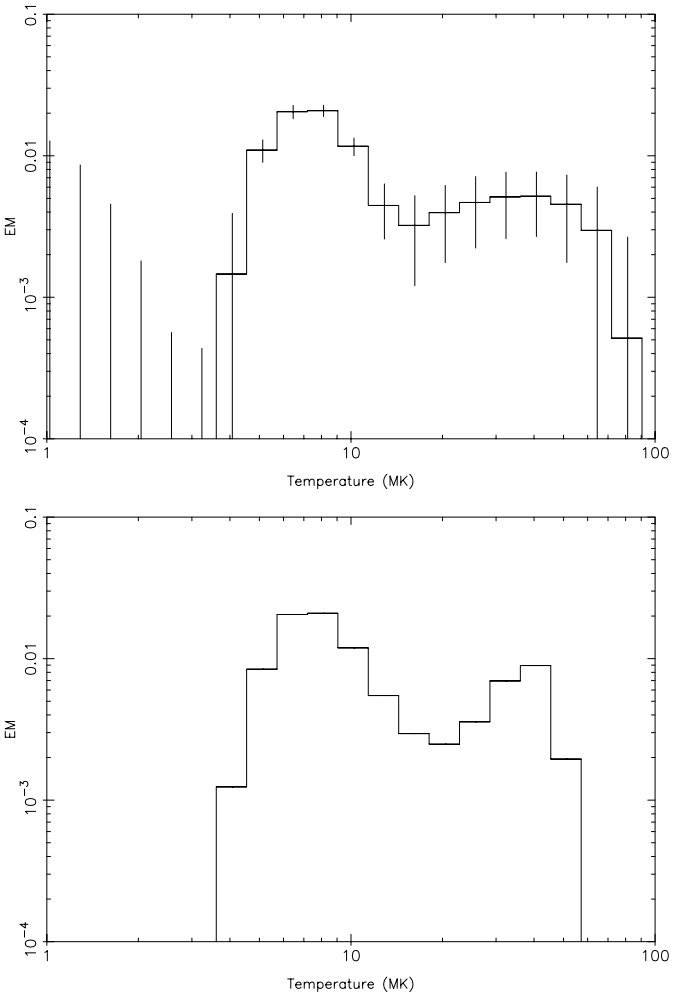

Fig. 3. Emission measure $EM (= n_e n_H V$ per logarithmic temperature bin) of WR 25 derived from the RGS and EPIC-MOS spectra in units of 10^{58} cm^{-3}. *Top:* the regularization method. *Bottom:* a polynomial fit of order 8.

4. A search for variability

As pointed out above, WR 25 may be a long-period binary. In this case, we might expect variations of its X-ray flux and/or spectral shape with the orbital phase. In a binary system consisting of two stars with strong winds, at least part of its X flux should be produced by the wind-wind collision (Prilutskii & Usov 1976). It may display phase-locked variability either as a consequence of the changing wind opacity along the line of sight towards the shock or as a result of the changing orbital separation in an eccentric binary.

In order to study this potential variability, we retrieved all available archival spectral data for WR 25 from *ROSAT*, *ASCA* (only SIS0 and SIS1 data, see below), and *XMM-Newton* public archives. Table 5 lists the log of these observations. For completeness, we added the relevant information for our current *XMM-Newton* observations.

4.1. Data reduction

As one of the primary goals of this archival study was to obtain a light curve, we had to make sure that the data were extracted and analyzed in as uniform and consistent way as possible. This includes using appropriate extraction apertures (large enough to include most of the PSF yet not to degrade signal-to-noise ratio and to avoid contamination from nearby sources; the latter especially important for the *ASCA* data) as well as consistent models to fit the spectra. Since the spectral characteristics and sensitivity of the three instruments are very different, the only way to get consistent fluxes is through fitting the spectra and calculating the model fluxes.

We retrieved the *ROSAT*-PSPC screened event files from the ARNIE database at Leicester University. The source spectra were extracted from an aperture 1′ in radius. The *ROSAT*-PSPC has an on-axis resolution of 20″ (PSF-FWHM) and WR 25 is a rather isolated source that lies well inside the inner ring of the wire mesh. The background spectra were extracted from an annular region centered on the source and with an inner radius of 1′ and outer radius of 2′.

The *ASCA* screened event files were retrieved from the same archive (only BRIGHT-mode data were used, as BRIGHT2-mode data represented a negligible fraction of all data available). The major problem with these data is low *ASCA* spatial resolution, which leads to contamination of WR 25 spectra from nearby η Car and the weaker but even more nearby O3V+O8V binary HD 93205 (see Fig. 1; Tsuboi et al. 1997, Fig. 1c). For GIS detectors, wherever one chooses the background extraction area, the background seems to be strongly contaminated by the nearby sources. This results in a GIS flux for WR 25 varying by more than 50% depending on the

Table 5. Log of archival and present observations of WR 25.

obs. no.	instrument	observation ID	observation date	MJD[a]	exposure (s)	total duration (s)
1	*ROSAT*-PSPCB	rp200108n00	1991, Dec. 15	48605.41	1610	2839
2	*ROSAT*-PSPCB	rp900176n00	1992, Jun. 12	48785.94	24 321	225 050
3	*ROSAT*-PSPCB	rp201262n00	1992, Aug. 09	48843.93	5665	42 858
4	*ROSAT*-PSPCB	rp900176a01	1992, Dec. 15	48971.73	14 544	2 096 652
5	*ASCA*-SIS0+SIS1	20018000	1993, Aug. 24	49223.76	30 048	74260
6	*ASCA*-SIS0+SIS1	26033000	1997, Jan. 24	50806.90	37 712	113 184
7	*XMM-Newton*-MOS1+PN[b]	0112580601	2000, Jul. 26	51751.71	31 600[c]	36 604
8	*XMM-Newton*-MOS1+PN[b]	0112580701	2000, Jul. 27	51753.50	9700[c]	12 572
9	*XMM-Newton*-MOS1+MOS2+PN	0112560101	2001, Jun. 25	52085.79	23 900[c]	36 994
10	*XMM-Newton*-MOS1+MOS2+PN	0112560201	2001, Jun. 28	52088.81	27 500[c]	38 506
11	*XMM-Newton*-MOS1+MOS2+PN	0112560301	2001, Jun. 30	52090.70	32 600[c]	37 474
12	*XMM-Newton*-RGS1+RGS2+MOS1	0112560201	2001, Jun. 28	52088.81	25 300[c]	38 506
13	*XMM-Newton*-RGS1+RGS2+MOS1	0112560301	2001, Jun. 30	52090.70	33 300[c]	37 474

[a] Exposure start.
[b] MOS2 was in "small window mode", with WR 25 close to the edge of the central CCD, which renders the data unusable.
[c] Some exposure time was lost due to (solar) high soft proton rate. Average exposure time is shown here, individual exposures for MOS1, MOS2, PN, RGS1, RGS2 are slightly different.

Table 6. Spectral fitting and X-ray fluxes at Earth for archival and *XMM*-EPIC data of WR 25.

obs.	$N_1^{\rm H}$	$N_2^{\rm H}$	kT_1	kT_2	$\chi^2_{\rm red}$	n.p.[b]	$f_{\rm x}$ (10^{-12} erg s^{-1} cm^{-2})		
no.	(10^{22} cm^{-2})		(keV)				[0.5–2.4 keV]	[2.4–10.0 keV]	[0.5–10.0 keV]
1	$1.03^{+0.32}_{-0.32}$	-	$0.42^{+0.25}_{-0.25}$	-	13.55/19	0.63	$2.13^{+0.26}_{-0.92}$	-	-
2	$0.91^{+0.10}_{-0.10}$	-	$0.56^{+0.10}_{-0.10}$	-	17.94/19	0.33	$2.14^{+0.18}_{-0.24}$	-	-
3	$0.96^{+0.19}_{-0.18}$	-	$0.52^{+0.17}_{-0.14}$	-	17.20/19	0.37	$2.67^{+0.33}_{-0.51}$	-	-
4	$0.95^{+0.11}_{-0.14}$	-	$0.56^{+0.14}_{-0.09}$	-	17.55/19	0.35	$2.36^{+0.29}_{-0.14}$	-	-
5	$1.05^{+0.33}_{-0.33}$	$0.48^{+0.42}_{-0.42}$	$0.71^{+0.22}_{-0.22}$	$2.58^{+0.78}_{-0.78}$	406/647	1.00	$1.73^{+1.59}_{-0.77}$	$1.46^{+0.72}_{-0.71}$	$3.19^{+2.31}_{-1.48}$
6	$0.63^{+0.12}_{-0.12}$	0.41[a]	$0.79^{+0.13}_{-0.13}$	$2.30^{+0.44}_{-0.44}$	397/648	1.00	$2.41^{+0.42}_{-0.45}$	$1.52^{+0.50}_{-0.98}$	$3.93^{+0.95}_{-1.43}$
7	$0.68^{+0.03}_{-0.02}$	$0.41^{+0.05}_{-0.04}$	$0.62^{+0.02}_{-0.01}$	$3.13^{+0.13}_{-0.20}$	1065/990	0.04	$2.86^{+0.03}_{-0.03}$	$1.82^{+0.05}_{-0.05}$	$4.68^{+0.07}_{-0.07}$
8	$0.68^{+0.05}_{-0.05}$	$0.41^{+0.10}_{-0.06}$	$0.60^{+0.03}_{-0.04}$	$2.98^{+0.41}_{-0.31}$	635/607	0.16	$2.79^{+0.05}_{-0.06}$	$1.81^{+0.06}_{-0.11}$	$4.59^{+0.10}_{-0.14}$
9	$0.70^{+0.02}_{-0.02}$	$0.43^{+0.04}_{-0.04}$	$0.62^{+0.02}_{-0.01}$	$2.65^{+0.14}_{-0.13}$	1398/1325	0.06	$2.42^{+0.03}_{-0.03}$	$1.43^{+0.03}_{-0.04}$	$3.85^{+0.04}_{-0.06}$
10	$0.71^{+0.02}_{-0.02}$	$0.38^{+0.08}_{-0.04}$	$0.62^{+0.01}_{-0.02}$	$3.01^{+0.19}_{-0.19}$	1398/1242	0.0008	$2.42^{+0.03}_{-0.02}$	$1.49^{+0.03}_{-0.04}$	$3.92^{+0.04}_{-0.07}$
11	$0.69^{+0.02}_{-0.03}$	$0.39^{+0.04}_{-0.03}$	$0.61^{+0.02}_{-0.01}$	$2.72^{+0.13}_{-0.12}$	1408/1357	0.135	$2.45^{+0.02}_{-0.03}$	$1.52^{+0.03}_{-0.04}$	$3.97^{+0.04}_{-0.05}$
12	$0.77^{+0.06}_{-0.05}$	$0.24^{+0.08}_{-0.07}$	$0.61^{+0.02}_{-0.03}$	$2.83^{+0.28}_{-0.48}$	643/619	0.244	$2.72^{+0.27}_{-0.27}$	$1.75^{+0.18}_{-0.18}$	$4.47^{+0.45}_{-0.45}$
13	$0.63^{+0.05}_{-0.05}$	$0.32^{+0.06}_{-0.05}$	$0.60^{+0.02}_{-0.02}$	$2.57^{+0.27}_{-0.26}$	727/613	0.001	$2.72^{+0.25}_{-0.25}$	$1.81^{+0.17}_{-0.17}$	$4.53^{+0.42}_{-0.42}$

[a] Signal-to-noise ratio in the hard part of the spectrum for this observation is so low that no reliable column density can be found. Thus, we fixed it at a value similar to that derived from *XMM-Newton* spectra.
[b] n.p.: null hypothesis probability, i.e., the probability that purely random deviations of the data from the model would result in obtained or higher value of $\chi^2_{\rm red}$.

Table 7. Average absorbed and unabsorbed X-ray luminosities of WR 25 for the three missions *ROSAT*, *ASCA* and *XMM-Newton*. The absorbed X-ray luminosity is derived from the X-ray fluxes (Table 6) using the adopted distance of WR25. The unabsorbed X-ray luminosity is the X-ray luminosity of WR25 just outside the absorbing wind, thus only corrected for interstellar absorption.

observatory	MJD_{av}	L_x (10^{32} erg s^{-1}) for $d = 3.24$ kpc		
		[0.5–2.4 keV]	[2.4–10.0 keV]	[0.5–10.0 keV]
		absorbed ($N_H = 0$)		
ROSAT (1-4)	48802	28.7 ± 4.9	-	-
ASCA (5-6)	50015	30.7 ± 11.2	19.2 ± 9.2	48.6 ± 19.9
XMM-Newton (7-11)	51954	31.8 ± 1.2	19.4 ± 0.9	50.9 ± 1.8
XMM-Newton (12-13)	52089	34.3 ± 3.4	22.4 ± 2.2	56.5 ± 5.6
		unabsorbed ($N_H = 3.5\times10^{21}$ cm^{-2})		
ROSAT (1-4)	48802	55.5 ± 4.9	-	-
ASCA (5-6)	50015	46.0 ± 10.2	19.4 ± 0.4	65.5 ± 10.7
XMM-Newton (7-11)	51954	63.4 ± 2.5	20.9 ± 1.1	83.8 ± 3.5
XMM-Newton (12-13)	52089	59.0 ± 4.2	23.9 ± 1.7	83.0 ± 5.9

background selection. For these reasons, we decided not to use the GIS data in the current analysis. Different CCDs of the two SIS instruments have difference responses. For this reason the source spectra for SIS0 and SIS1 data were extracted from a part of a circular aperture 3′ in radius lying within a single CCD frame, while the background was extracted from a rectangular area within the same CCD frame. As in the 1997 *ASCA* observation WR 25 is located near the edge of the field of view, the flux obtained for this observation may be unreliable. As a consistency check, we compared our results for the 1993 *ASCA* observation with that of Skinner et al. (1995). Our absorbed SIS1 flux in the 0.5–4 keV band as well as model parameters are practically identical to those given by Skinner et al.

The first two *XMM*-EPIC MOS1, MOS2 and PN data sets shown in Table 5 were retrieved from the public *XMM-Newton* data archive. Only "good" events (e.g., with pattern 0–12 for the MOS, etc., see Turner et al. 2001) were considered. No indication of pile-up was found in the data. Only good-time intervals with low level of the soft proton background were included in the analysis. We adopted the most up-to-date (July 2002) redistribution matrices provided by the EPIC instrument teams and used SAS to build the appropriate ancillary response file for each observation. As the goal of this section is to get accurate estimates of the flux, we used a relatively large source extraction aperture equal to 1′ in radius; the background spectra were extracted from an annulus centered on the source region (inner radius of 1′, outer radius 85″).

In the first two *XMM* data sets from Table 5, η Car was the primary target, situated in the center of the field of view. Consequently, WR 25 was offset from the center by some 7′. This may lead to systematic errors of the derived flux due to: (*i*) inaccuracy of the Point Spread Function of the X-ray telescopes; and (*ii*) a calibration error in the vignetting.

According to the in-flight calibration of the EPIC-PSF (*XMM* report CAL-TN-0018-2-0), a reliable correction for the encircled energy fraction (EEF) at the off-axis angle 7′ can only be done with reasonable accuracy (better than 5% at energies below ∼1.5 keV for MOS1, MOS2 and 4 keV for PN). Above these limits, the error may be as large as 20% or calibration is simply non-existent (e.g., at $E > 4$ keV for PN).

For this reason we did not apply the EEF correction to the extracted fluxes in data sets 7–11. This must allow one to obtain more reliable comparison between *XMM* fluxes of WR 25 in data sets 7, 8 and 9–11 provided that the extraction aperture is large enough. Indeed, e.g. for on-axis observations with MOS the EEF within the aperture $R = 1'$ exceeds 92% depending on energy. We may expect a not very different fraction for the 7′ offset angle. Note that while formally speaking the current parameterization of the EEF at high energies and large off-axis angles is unreliable, according to it, the difference in the EEF corrections on-axis and 7′ off-axis for our aperture size does not exceed 1% for MOS1, MOS2 and 2% for PN.

In data sets 12 and 13 (WR 25 on-axis) we did apply the EEF, to estimate its influence on the resulting fluxes compared to the data sets 9–11 (10, 11 are same observations as 12, 13, although different sets of instruments).

As for the second source of error, we were advised by the *XMM*-Helpdesk that an uncertainty in the position of the optical-axis used within the SAS is currently giving an error in the flux, estimated to be about 3%, 10%, and 8% for MOS1, MOS2, and PN respectively at 7′ off-axis for an energy of 4.5 keV. There is a small energy dependence on the above values with lower energies being affected less. There is also a 2–4% error introduced by the same effect on the on-axis measurements.

We conclude that the error of the WR 25 absolute flux for *XMM* data sets 12, 13 (Table 5, WR 25 on-axis) should not exceed ∼5–7%. The fluxes in data sets 7–11 may be

systematically underestimated by some 6–10% due to the lack of the EEF-correction. Apart from this systematic error, the error of the flux measured within our $R = 1'$ aperture should not exceed ∼5–7% for the data sets 9–11 and may be somewhat larger for the data sets 7, 8.

4.2. Spectral shape and flux variations

All data were analyzed using the XSPEC software (version 11.2.0). We fixed chemical abundances at values obtained in the previous section. For *XMM* and *ASCA* data we used a two-temperature thermal plasma MEKAL model (Mewe et al. 1985; Kaastra 1992) allowing distinct column densities for both components. The column densities obtained in the best-fit models are comparable or larger than the equivalent H I column density ($N_{\rm H} = 3.5 \pm 1.1 \times 10^{21}$ cm^{-2}, Diplas & Savage 1994). The *ROSAT* sensitivity range (0.5–2.4 keV) does not justify using a two-temperature model, so these data were fit with a single-temperature absorbed MEKAL model. The fitted model parameters are shown in Table 6 (including the reduced χ^2 value and the null hypothesis probability of the fits). Table 6 lists the model fluxes integrated over three energy ranges (0.5–2.4 keV, 2.4–10.0 keV, and 0.5–10.0 keV).

It can be seen indeed that the EEF-corrected fluxes in data sets 12 and 13 are about 10% higher than the fluxes in data sets 9–11. On the other hand, these differences may also reflect calibration uncertainties between EPIC and RGS. The light curves in three energy bands are shown in Fig. 4 (fluxes from data sets 7–11 are plotted for *XMM*).

From Table 6 it is clear that the spectral shape of WR 25 has not changed much in the course of 10 years. The column density at the *ROSAT* epoch is somewhat larger than that at the *XMM-Newton* epoch, but considering the errors of the former the results are quite compatible. Also, part of the difference in $N_{\rm H}$ may come from the absence of the high-temperature component in our modeling of the *ROSAT* data. The *ASCA* data (especially in the second observation) have very poor signal-to-noise ratio, especially in the high energy part. This explains "too good to be true" χ^2 values and somewhat deviating model parameters.

In the relatively short history of X-ray astronomy, the X-ray flux of WR 25 has not shown strong variability, as is evident from Table 6 and Fig. 4. The *XMM* fluxes obtained on time interval of about 1 year differ by some 15%. However, provided that the calibration at high energies and large off-axis angles is not very good (see above), this difference may be related to the calibration uncertainties. On the other hand, the flux differences for the soft and hard bands are quite consistent; recall that the calibration for low energies is better at large off-axis angles[3]. We conclude that we have not yet found spectral shape or flux variations providing a clear indication of the suspected binarity of WR 25. This could indicate a very-long period orbit, e.g., like those of WR 146, $P \approx 550$ yr, or even WR 147, $P \approx 1350$ yr (Setia Gunawan et al. 2000, 2001; van der Hucht et al. 2002a), and/or a circular orbit, although even a circular orbit could induce variability due to inclination-dependent line-of-sight absorption.

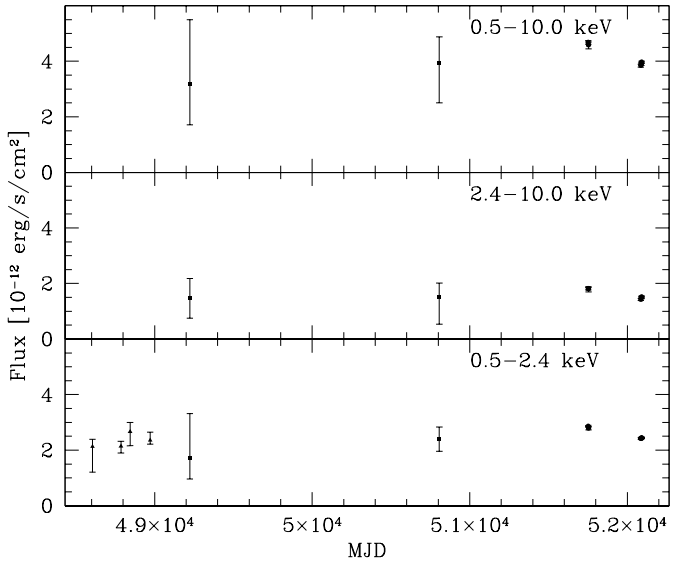

Fig. 4. *ROSAT*/*ASCA*/*XMM* X-ray light curves of WR 25. Triangles: *ROSAT*; squares: *ASCA*; and dots: *XMM*. Note the, relatively, very small error bars for the *XMM* fluxes.

4.3. X-ray luminosity

Using X-ray fluxes of WR 25 obtained in previous subsections we determined the unabsorbed luminosities of WR 25 for every mission/epoch. We did this by removing the interstellar column density $N_{\rm H}^{\rm ISM} = 3.5 \times 10^{21}$ cm^{-2} from the best model fits and computing the resulting model fluxes. The luminosities were then calculated from these "unabsorbed" fluxes for the assumed distance to WR 25 $d = 3.24$ kpc. To estimate the errors of the luminosities we simulated a synthetic spectrum for each instrument (*ROSAT*, *XMM*, *ASCA*) including the effect of photon noise, using the best fit models corrected for the ISM column density. The errors on the flux for these simulated data can then be evaluated in a standard way. The average unabsorbed X-ray luminosities of WR 25 for these three missions are shown in Table 7.

Seward & Chlebowski (1982) and Pollock (1987) reported very different X-ray luminosities of WR 25 (see Sect. 1) using the same *Einstein*-IPC (0.2–4.0 keV) data. The difference between these authors apparently comes from different use of the (same) data: Seward & Chlebowski used the *measured* count rate in the whole IPC (0.2–4.0 keV) energy range while Pollock only used the hard band (0.8–4.0 keV) and *extrapolated* the hard band count rate to the soft band assuming a 1 keV thermal model. Doing so, he neglected internal absorption in the wind of WR 25 which is evident from our *XMM* study. In a 1 keV thermal model without wind absorption we would expect a significant number of counts in the soft IPC-band. Remarkably, though, the *observed* count rates are almost identical: 0.14 ± 0.02 counts/s for Seward & Chlebowski and 0.13 ± 0.02 count/s for Pollock.

[3] Note that the XMM flux errors in Table 6 and in Fig. 4 do not account for systematic vignetting errors and thus are underestimated.

We used our best-fit model 10 (Table 6) to simulate a synthetic *Einstein*-IPC spectrum and then get the count rates. The simulated IPC count rate in the 0.2 – 4.0 keV band is 0.12 counts s^{-1}, which, in view of all uncertainties involved, is in excellent agreement with the measured value. The simulated count rate in the 0.8–4.0 keV band is 0.11 counts s^{-1}, indeed very close to the total count rate due to the above mentioned wind absorption.

We conclude that the X-ray luminosity of WR 25 at the *Einstein* epoch is consistent with the *XMM* L_x value.

5. The 6.4–6.7 keV Fe-complex: Evidence for colliding winds and thus binarity?

We measured the energy and the equivalent width of this complex by fitting a power law continuum plus a Gaussian to the spectrum extracted between 4.4 and 8.0 keV. The results are listed in Table 8. The given HJD (heliocentric Julian day) are corresponding to the middle of the exposures. No significant variability of the strength of the Fe-complex is detected between the four epochs.

In Table 9 we list the observations of the 6.4 keV Fe-emission line complex in WR 25 and other hot massive stars. We divided Table 9 in single stars and known binaries.

In fact, the temperature elevation associated with hydrodynamic shocks in the winds of single stars is usually not sufficient to produce a significant Fe Kα emission. On the other hand, in a wide binary system, the winds of the binary components collide with velocities close to v_∞ and hence the plasma in the wind interaction zone can be significantly hotter. These considerations suggest that the Fe-complex is a diagnostic for colliding-wind binaries with the Fe-complex originating in the hot plasma of the wind collision zone.

Not all observations listed in Table 9 were equally sensitive at 6.4–6.7 keV. And in the case of the widest listed binary, WR 147, the binary-component separation (~417 AU, Setia Gunawan et al. 2000) may be too large to generate a visible Fe-complex in the peak of the collision cone, while the non-thermal radio emission originating in the wake of the collision cone is coming from a much larger volume. Nonetheless, Table 9 shows that the observed binaries have a larger fraction showing the Fe-complex than single stars do. Because of the small number of available data this is, of course, not statistically significant, but at least a stimulating indication. This implies that the WR object WR 110 and the O-type objects HD 93129A, HD 93250 and θ^1 Ori C could also be colliding-wind binaries. Incidentally, HD 93129A has recently proven to be a 60 mas (~200 AU at $d = 3.24$ kpc) visual binary (Walborn 2003).

6. Implications of results

In understanding the nature of WR 25, one very important aspect is clearly the L_x/L_{bol} value of WR 25: for the first time we are in the position to provide a meaningful and accurate luminosity and to estimate how over-luminous WR 25 really is. In fact, using the ISM-corrected luminosities and the L_{bol} value from Table 1 yields $L_x/L_{bol} = 2.37\times10^{-6}$ (i.e., $\log(L_x/L_{bol}) = -5.62$). While this ratio is large, Fig. 1 in Wessolowski (1996) shows that there may be other presumably single WN stars that have similar ratios. Of course, one could argue that these other systems are less well known and may also be yet unidentified binaries. Since WR 25 is the least extreme WN star, it is also instructive to compare its L_x/L_{bol} ratio with the relation for O-type stars given by Berghöfer et al. (1997): the L_x for WR 25 we derived in this study is more than a factor of 10 larger than the value expected from their relation for O-type stars.

There are a number of clues about the multiplicity of WR 25: on the plus side, we have (*i*) the large X-ray luminosity (see above), well in excess of what is expected (even accounting for the dispersion in the empirical L_x vs. L_{bol} relations), and (*ii*) the high-temperature component: how could such a high temperature emission be produced in the wind of a single star? On the minus side, we have (*i*) the lack of short-term and long-term X-ray variability, and (*ii*) the lack of variability-evidence for binarity at other wavelengths, except for the optical polarization-variability found by Drissen et al. (1992). The first counter-argument could be overcome by assuming that WR 25 is either a (very) long-period binary or a system that is nearly seen pole on. In any case, long-term monitoring of WR 25 over a broad wavelength range will be instrumental to clarify its nature.

Table 8. Properties of the Fe-complex at ~6.7 keV in the *XMM* spectrum of WR 25.

rev. #	HJD 2 450 000+	line energy (keV)	*EW* (keV)
115	1751.908	6.65 ± 0.02	0.88
116	1753.562	6.70 ± 0.03	0.82
284	2089.055	6.65 ± 0.02	0.70
285	2090.914	6.65 ± 0.02	0.78

7. Summary

The object WR 25 (WN6h) has been observed by *XMM*-RGS and -EPIC. A broad temperature range associated with the X-ray radiation has been established by multi-temperature fitting and DEM modeling of the spectra between 5 and 60 MK with maxima around 7.5 and 35 MK. In this temperature range the total emission measure is about 9.5×10^{56} cm^{-3}. Above 15 Å the radiation is absorbed by the dense wind around the WR star and no features are observed in that region. The data are consistent with two different N_H values: 7×10^{21} cm^{-2} and 3×10^{21} cm^{-2} for the two temperature components. We notice that the column density for the softer component is larger than the ISM value indicating that there is significant wind absorption.

No abundance anomalies have been noticed. For C and N no values could be obtained (we used fixed literature values) and all other elements were slightly subsolar (except S which was about solar).

The X-ray flux and spectral shape of WR 25 as measured by *ROSAT*, *ASCA*, and *XMM* do not show significant

Table 9. X-ray spectroscopy of O-type stars and WR stars and the occurrence of the 6.4–6.7 keV Fe emission-line complex.

star	HD/ other	spectral type[a]	P^a	d^a (kpc)	obser- vatory	T from X-rays T_1 (MK)	T_2 (MK)	6.4–6.7 keV Fe-complex observed	reference
spectroscopic binaries and suspected binaries:									
WR 6, EZ CMa	50896	WN4+?	3.76 d	0.97	*A*, *C*	7	35–49	yes	1, 2
WR 139	193576	WN5+O6III-V	4.21 d	1.90	*A*	7	23	yes	3
WR 25	93162	WN6h+O4f		3.24	*A*, *X*	7	32	yes	4, 5
WR 43c	97950C	WN6ha+?		7	*C*			yes	6
WR 147	AS 431	WN8h+O5-7I-II(f)	~1350 yr	0.65	*A*	12	>23	no	7
WR 140	193793	WC7+O4-5	7.94 yr	1.10	*G*, *A*	34		yes	3, 8
WR 11, γ^2 Vel	68273	WC8+O7.5III-V	78.53 d	0.26	*A*, *C*, *X*	~ 4 - ≳ 25		yes	9, 10, 11
η Car	93308	LBV+WR?	5.52 yr	3.24	*A*, *C*, *X*, *S*	< 8	54	yes	4, 12, 13, 14, 15, 16
Tr 16-179	93205	O3V+O8V	6.08 d	3.24	*X*			yes?	17
9 Sgr	164794	O4V((f$^+$))+?		1.52	*X*	~ 3	≳20	yes?	18
CD–58 3545	93403	O5.5I+O7V	15.09 d	3.24	*X*	3	12	no	19
V1036 Sco	159176	O6V+O7V	3.37 d	1.5	*X*	~ 2	~ 7	no	20
ι Ori	37043	O9III+B1III	29.13 d	0.45	*A*	1–7	7–36	yes?	21
δ Ori A	36486	O9.5II+B0.5III	5.73 d	0.36	*A*, *C*	~ 4		no	22, 23
supposedly single stars:									
WR 110	165688	WN5-6		1.28	*X*	6	≳ 35	yes	24
Tr 14-MJ198	93129A	O2If*		3.24	*X*			yes?	17
Tr 16-180	93250	O3V((f$^+$))		3.24	*X*			yes?	17
ζ Pup	66811	O4I(n)f		0.45	*C*, *X*	4–16		no	25, 26
θ^1 Ori C	37022	O6pe		0.45	*A*, *C*	9	~ 35	yes	27, 28, 29
λ Ori	36861J	O8III((f))		0.32	*A*	26		no	22
ζ Ori	37742	O9.7Ib		0.25	*A*, *C*	≳ 10		no	30, 31
τ Sco	149438	B0.2V		0.13	*A*, *X*, *C*	1–2	5–10[b]	no	32, 33, 34

Observatories: *A*: *ASCA*; *C*: *Chandra*; *G*: *Ginga*; *S*: *BeppoSAX*; *X*: *XMM-Newton*.
Notes: [a] WR star spectral types, periods and distances from van der Hucht (2001). [b] 3rd T-range: 30–40 MK.
yes?: 6.4–6.7 keV region has low S/N ratio, but indication of Fe-complex present.
References: 1) Skinner et al. (1998); 2) Skinner et al. (2002a); 3) Maeda et al. (1999); 4) Skinner et al. (1995); 5) this study; 6) Moffat et al. (2002); 7) Skinner et al. (1999); 8) Koyama et al. (1990); 9) Rauw et al. (2000); 10) Skinner et al. (2001); 11) Dumm et al. (2003); 12) Tsuboi et al. (1997); 13) Corcoran et al. (2001); 14) Pittard & Corcoran (2002); 15) Viotti et al. (2002); 16) Leutenegger et al. (2003); 17) Antokhin et al. in preparation; 18) Rauw et al. (2002a); 19) Rauw et al. (2002b); 20) De Becker et al. (2003); 21) Pittard et al. (2000); 22) Corcoran et al. (1994); 23) Miller et al. (2002); 24) Skinner et al. (2002b); 25) Kahn et al. (2001); 26) Cassinelli et al. (2001); 27) Yamauchi et al. (1996); 28) Schulz et al. (2000); 29) Schulz et al. (2001); 30) Waldron et al. (2003); 31) Waldron & Cassinelli (2001); 32) Cohen et al. (1997); 33) Mewe et al. (2003); 34) Cohen et al. (2003).

variations over the last decade, although the most accurate data, from *XMM*, show slight flux variability (~15%).

The presence of the Fe xxv emission-line complex at ~6.7 keV is argued as being indicative for colliding winds inside a WR+O binary system.

Acknowledgements. We are grateful to the calibration teams of the instruments on board *XMM-Newton*, and to the referee, Dr. Nicole St-Louis, for her constructive comments and suggestions. The SRON National Institute for Space Research is supported financially by NWO. IA acknowledges support from the Russian Foundation for Basic Research (grants 02-02-17524, 02-02-06591, 02-15-96553). The Liège team acknowledges support from the Fonds National de la Recherche Scientifique (Belgium), the PRODEX *XMM*-ом and *Integral* Projects and from contracts P4/05 and P5/36 "Pôle d'Attraction Interuniversitaire" (SSTC-Belgium). MG acknowledges support from the Swiss National Science Foundation (grant 2100-049343). This research has made use of the Digitized Sky Survey produced by STScI.

References

Anders, E., & Grevesse, N. 1989, Geochim. Cosmochim. Acta, 53, 197
Baum, E., Hamann, W.-R., Koesterke, L., & Wessolowski, U. 1992, A&A, 266, 402
Berghöfer, T. W., Schmitt, J. H. M. M., Danner, R., & Cassinelli, J. P. 1997, A&A, 322, 167
Cassinelli, J. P., Miller, N. A., Waldron, W. L., MacFarlane, J. J., & Cohen, D. H. 2001, ApJ, 544, L55
Chapman, J. M., Leitherer, C., Koribalski, B., Bouter, R., & Story, M. 1999, ApJ, 518, 890
Cherepashchuk, A. M. 1976, Pis'ma Astron. Zh., 2, 356 (= Sov. Astron. Lett., 2, 138)
Cohen, D. H., Cassinelli, J. P., & Waldron, W. L. 1997, ApJ, 488, 397

Cohen, D. H., de Messières, G., Macfarlane, J. J., et al. 2003, ApJ, 586, 495
Conti, P. S., Niemela, V. S., & Walborn, N. R. 1979, ApJ, 228, 206
Corcoran, M. F., Waldron, W. L., MacFarlane, J. J., Chen, W., & Pollock, A. M. T. 1994, ApJ, 436, L95
Corcoran, M. F., Swank, J., Rawley, G., et al. 1995, in ed. V. P. Niemela, N. Morrell, & A. Feinstein, The η Carinae Region: a Laboratory of Stellar Evolution, RMAA-SC2, 97
Corcoran, M. F., Swank, J. H., Petre, R., Ishibashi, K., & Davidson, K. 2001, ApJ, 562, 1031
Corcoran, M. F. 2003, in ed. K. A. van der Hucht, A. Herrero, & C. Esteban, A Massive Star Odyssey, from Main Sequence to Supernova, Proc. IAU Symp. 212 (San Francisco: ASP), 130
Crowther, P. A., Hillier, D. J., & Smith, L. J. 1995a, A&A, 293, 403
Crowther, P. A., Smith, L. J., Hillier, D. J., & Schmutz, W. 1995b, A&A, 293, 427
Cruddace, R., Paresce, F., Bowyer, S., & Lampton, M. 1974, ApJ, 187, 497
De Becker, M., Rauw, G., Pittard, J. M., Stevens, I. R., & Gosset, E. 2003, in preparation
Dessart, L., & Owocki, S. P. 2002, A&A, 383, 1113
Diplas, A., & Savage, B. D. 1994, ApJS, 93, 211
Drissen, L., Robert, C., & Moffat, A. F. J. 1992, ApJ, 386, 288
Dumm, Th., Güdel, M., Schmutz, et al. 2003, in New Visions of the X-ray Universe in the *XMM-Newton* and *Chandra* Era, Proc. Int. Workshop, Noordwijk, ed. F. Jansen, & TBD (The Netherlands), 26–30 November 2001, ESA SP-488, in press
Grevesse, N., & Sauval, A. J. 1998, in ed. C. Frölich, M. C. E. Huber, S. K. Solanki, & R. von Steiger, Solar Composition and its Evolution – From Core to Corona, Space Sci. Rev., 85, 161
Grevesse, N., & Sauval, A. J. 1999, A&A, 347, 348
Feldmeier, A., Kudritzki, R.-P., Palsa, R., Pauldrach, A. W. A., & Puls, J. 1997a, A&A, 320, 899
Feldmeier, A., Puls, J., & Pauldrach, A. W. A. 1997b, A&A, 322, 878
Hamann, W.-R., & Koesterke, L. 1998, A&A, 333, 251
den Herder, J. W., Brinkman, A. C., Kahn, S. M., et al. 2001, A&A, 365, L7
van der Hucht, K. A., Conti, P. S., Lundström, I., & Stenholm, B. 1981, Space Sci. Rev., 28, 227
van der Hucht, K. A. 1992, A&A Rev., 4, 123
van der Hucht, K. A., Williams, P. M., Spoelstra, T. A. Th., & de Bruyn, A. G. 1992, in Non-isotropic and Variable Outflows from Stars, Proc. STScI Workshop, ed. L. Drissen, C. Leitherer, & A. Nota, ASP-CS, 22, 253
van der Hucht, K. A. 2001, New Astron Rev., 45, 135
van der Hucht, K. A. 2002b, in Multifrequency Behaviour of High Energy Cosmic Sources, Proc. Frascati Workshop 2001, Vulcano (Italia), 21–26 May 2001, ed. F. Giovanelli, & L. Sabau-Graziati, Mem. Soc. Astron. Italia, 73 (4), 822
van der Hucht, K. A., Setia Gunawan, D. Y. A., Williams, P. M., de Bruyn, A. G., & Spoelstra, T. A. Th. 2002, in Interacting Winds from Massive Stars, Proc. Int. Workshop, Les Îles-de-la-Madeleine (Québec, Canada) 10–14 July 2000, ed. A. F. J. Moffat, & N. St-Louis, ASP-CS260, 297
Ignace, R., Oskinova, L. M., & Foullon, C. 2000, MNRAS, 318, 214
Ignace, R., & Gayley, M. 2002, ApJ, 568, 954
Jansen, F., Lumb, D. H., Altieri, B., et al. 2001, A&A, 365, L1
Kaastra, J. S. 1992, An X-ray Spectral Code for Optically Thin Plasmas, SRON-Leiden Internal Report
Kaastra, J. S., Mewe, R., & Nieuwenhuijzen, H. 1996a, in UV and X-ray Spectroscopy of Astrophysical and Laboratory Plasmas, ed. K. Yamashita, & T. Watanabe (Tokyo: Universal Academy Press, Inc.), 411 (SPEX)
Kaastra, J. S., Mewe, R., Liedahl, D. A., et al. 1996b, A&A, 314, 547
Kahn, S. M., Leutenegger, M. A., Cottam, J., et al. 2001, A&A, 365, L312
Kelly, R. L. 1987, tomic and Ionic Spectral Lines below 2000 Angströms: Hydrogen through Krypton, J. Phys. Chem. Ref. Data 16, Suppl. 1
Koyama, K., Kawada, M., & Takano, S. 1990, PASJ, 42, L1
Leitherer, C., Chapman, J. M., & Koribalski, B. 1995, ApJ, 450, 289
Leutenegger, M. A., Kahn, S. M., & Ramsay, G. 2003, ApJ, 585, 1015
Lucy, L. B., & White, R. L. 1980, ApJ, 241, 300
Lucy, L. B. 1982, ApJ, 255, 286
Luo, D., McCray, R., & Mac Low, M.-M. 1990, ApJ, 362, 267
Maeda, Y., Koyama, K., Yokogawa, J., & Skinner, S. 1999, ApJ, 510, 967
Massey, P., & Johnson, J. 1993, AJ, 105, 980
Mewe, R., Gronenschild, E. H. B. M., & van den Oord, G. H. J. 1985, A&AS, 62, 197 (MEKAL)
Mewe, R., Kaastra, J. S., & Liedahl, D. A. 1995, Legacy 6, 16 (MEKAL)
Mewe, R., Raassen, A. J. J., Cassinelli, J. P., et al. 2003, A&A, 398, 203
Miller, N. A., Cassinelli, J. P., Waldron, W. L. MacFarlane, J. J., & Cohen, D. H. 2002, ApJ, 577, 951
Moffat, A. F. J. 1978, A&A, 68, 41
Moffat, A. F. J., & Niemela, V. S. 1984, ApJ, 284, 631
Moffat, A. F. J., Corcoran, M. F., Stevens, I. R., et al. 2002, ApJ, 573, 191
Niemela, V. P., Morrell, N., & Feinstein, A. (eds.) 1995, The η Carinae Region: a Laboratory of Stellar Evolution, RMAA-SC, 2
Owocki, S. P., & Gayley, K. G. 1995, ApJ, 454, L145
Owocki, S. P., & Gayley, K. G. 1999, in Wolf-Rayet Phenomena in Massive Stars and Starburst Galaxies, ed. K. A. van der Hucht, G. Koenigsberger, & P. R. J. Eenens, Proc. IAU Symp. 193 (San Francisco: ASP), 157
Owocki, S. P., & Cohen, D. H. 1999, ApJ, 520, 833
Phillips, K. J. H., Mewe, R., & Harra-Murnion, L. K., et al. 1999, A&AS, 138, 381
Pittard, J. M., & Stevens, I. R. 1997, MNRAS, 292, 298
Pittard, J. M., Stevens, I. R., Corcoran, M. F., et al. 2000, MNRAS, 319, 137
Pittard, J. M., & Corcoran, M. F. 2002, A&A, 383, 636
Pittard, J. M., & Stevens, I. R. 2002, A&A, 388, L20
Pollock, A. M. T. 1987, ApJ, 320, 283
Pollock, A. M. T. 1989, ApJ, 347, 409
Pollock, A. M. T. 1991, in Wolf-Rayet Stars and Interrelations with Other Massive Stars in Galaxies, ed. K. A. van der Hucht, & B. Hidayat, Proc. IAU Symp. 143 (Dordrecht: Kluwer), 105
Pollock, A. M. T. 1995, in Wolf-Rayet Stars: Binaries, Colliding Winds, Evolution, ed. K. A. van der Hucht, & P. M. Williams, Proc. IAU Symp. 163 (Dordrecht: Kluwer), 429
Pollock, A. M. T., Haberl, F., & Corcoran, M. F. 1995, in Wolf-Rayet Stars: Binaries, Colliding Winds, Evolution, ed. K. A. van der Hucht, & P. M. Williams, Proc. IAU Symp. 163 (Dordrecht: Kluwer), 512
Pollock, A. M. T. 2002, Workshop High resolution X-ray spectroscopy with XMM-Newton and Chandra, Oct. 2002, MSSL
Prilutskii, O. F., & Usov, V. V. 1976, Astron. Zh., 53, 6 (= Sov. Astron., 20, 2)
Prinja, R. K., Barlow, M. J., & Howarth, I. D. 1990, ApJ, 361, 607 (*Erratum*: 1991, ApJ, 383, 466)
Rauw, G., Stevens, I. R., Pittard, J. M., & Corcoran, M. F. 2000, MNRAS, 316, 129
Rauw, G., Blomme, R., Waldron, W. L., et al. 2002a, A&A, 394, 993
Rauw, G., Vreux, J.-M., Stevens, I. R., et al. 2002b, A&A, 388, 552

Sanders, W. T., Cassinelli, J. P., Myers, R. V., & van der Hucht, K. A. 1985, ApJ, 288, 756
Setia Gunawan, D. Y. A., de Bruyn, A. G., van der Hucht, K. A., & Williams, P. M. 2000, A&A, 356, 676
Setia Gunawan, D. Y. A., de Bruyn, A. G., van der Hucht, K. A., & Williams, P. M. 2001, A&A, 368, 484
Seward, F. D., Forman, W. R., Giacconi, R., et al. 1979, ApJ, 234, L55
Seward, F. D., & Chlebowski, T. 1982, ApJ, 256, 530
Schulz, N. S., Canizares, C. R., Huenemoerder, D., & Lee, J. C. 2000, ApJ, 545, L139
Schulz, N. S., Canizares, C. R., Huenemoerder, D., et al. 2001, ApJ, 549, 441
Skinner, S. L., Nagase, F., Koyama, K., Maeda, Y., & Tsuboi, Y. 1995, in Wolf-Rayet Stars: Binaries, Colliding Winds, Evolution, ed. K. A. van der Hucht, & P. M. Williams, Proc. IAU Symp., 163 (Dordrecht: Kluwer), 471
Skinner, S. L., Itoh, M., & Nagase, F. 1998, New Astron., 3, 37
Skinner, S. L., Itoh, M., Nagase, F., & Zhekov, S. A. 1999, ApJ, 524, 394
Skinner, S. L., Güdel, M., Schmutz, W., & Stevens, I. R. 2001, ApJ, 558, L113
Skinner, S. L., Zhekov, S. A., Güdel, M., & Schmutz, W. 2002a, ApJ, 579, 764
Skinner, S. L., Zhekov, S. A., Güdel, M., & Schmutz, W. 2002b, ApJ, 572, 477
Smith, H. J. 1955, Southern Wolf-Rayet Stars, Thesis Harvard University, Cambridge, USA
Smith, L. F. 1968, MNRAS, 138, 109
Smith, L. F., Shara, M. M., & Moffat, A. F. J. 1996, MNRAS, 281, 163
Stevens, I. R., Blondin, J. M., & Pollock, A. M. T. 1992, ApJ, 386, 265
Strüder, L., Briel, U. G., Dennerl, K., et al. 2001, A&A, 365, L18
Thé, P. S., Bakker, R., & Tjin A Djie, H. R. E. 1980, A&A, 89, 209
Tsuboi, Y., Koyama, K., Sakano, M., & Petre, R. 1997, PASJ 49, 85
Turner, D. G., & Moffat, A. F. J. 1980, MNRAS, 192, 283
Turner, M. J. L., Abbey, A., Arnaud, M., et al. 2001, A&A, 365, L27
Viotti, R. F., Antonelli, L. A., Corcoran, M. F., et al. 2002, A&A, 385, 874
Walborn, N. R., Nichols-Bohlin, J., & Panek, R. J. 1985, International Ultraviolet Explorer Atlas of O-type Spectra from 1200 to 1900 Å, NASA RP-1155
Walborn, N. R., Howarth, I. D., Lennon, D. J., et al. 2002, AJ, 123, 2754
Walborn, N. R. 2003, in A Massive Star Odyssey, from Main Sequence to Supernova, ed. K. A. van der Hucht, A. Herrero, & C. Esteban, Proc. IAU Symp. No. 212 (San Francisco: ASP), p. 13
Waldron, W. L., Corcoran, M. F., Drake, S. A., & Smale, A. P. 1998, ApJS, 118, 217
Waldron, W. L., & Cassinelli, J. P. 2001, ApJ, 548, L45
Waldron, W. L., Corcoran, M. F., & Kitamoto, S. 2003, in preparation
Wessolowski, U. 1996, in Röntgenstrahlung from the Universe, ed. H. U. Zimmermann, J. E. Trümper, & H. Yorke, Proc. Wurzburg Conf., September 1995, MPE Rep., 263, 75
White, R. L., & Long, K. S. 1986, ApJ, 310, 832
Williams, P. M., van der Hucht, K. A., Pollock, A. M. T., et al. 1990, MNRAS, 243, 662
Willis, A. J., & Crowther, P. A. 1996, in Wolf-Rayet Stars in the Framework of Stellar Evolution, ed. J.-M. Vreux, A. Detal, D. Fraipont-Caro, E. Gosset, & G. Rauw, Proc. 33rd Liège Int. Astroph. Coll. (Liège: Univ. of Liège), p. 109
Yamauchi, S., Koyama, K., Sakano, M., & Okada, K. 1996, PASJ 48, 719